Nanostructures

DOI: 10.1002/anie.201208901

Palladium-Based Nanostructures with Highly Porous Features and Perpendicular Pore Channels as Enhanced Organic Catalysts**

*Xiaoqing Huang, Yongjia Li, Yu Chen, Enbo Zhou, Yuxi Xu, Hailong Zhou, Xiangfeng Duan, and Yu Huang**

During the past decades, noble-metal nanostructures (such as, Pt, Pd, and Au)[1] have attracted considerable research interest in both fundamental studies and various practical applications because of their unique catalytic, electronic, photonic, and sensing properties.[2] However, because of their high cost and limited reserves, it is urgent to reduce their required usage in such applications.[3] Fortunately, theoretical predictions and various experimental results have suggested that the performance of noble-metal nanocrystals is highly dependent on their morphology.[4] The efficiency and selectivity of the metal nanocrystals toward a specific catalytic process can be optimized by controlling their structures, which has triggered great efforts in the development of controllable synthesis.[4] Achieving desirable structures of noble-metal nanocatalysts can endow them with superior catalytic performance and improved efficiency based on their mass.[5]

More recently, special attention has been paid to the fabrication of metallic nanocrystals with highly dendritic/porous structures.[6] Owing to their high surface area and rich edge/corner atoms, the dendritic/porous nanostructures are highly favorable for high catalytic performance and decreased noble-metal consumption.[6] For instance, because of a high surface area and highly active surface sites, the Pt-Pd bimetallic nanodendrites show much higher oxygen reduction reaction (ORR) activity compared with commercial Pt catalysts.[1b] Dendritic/porous metal nanostructures in a wide range of compositions, such as Pt, Pd, PtPd, and PtAu, have been prepared by the wet-chemical method.[7] However, it should be noted that the branches in all the reported dendritic/porous nanostructures are random and the branch sizes are still relatively large. Nevertheless, the presence of perpendicular pore channels in the porous nanostructures is essential for high accessibility to the adsorbed species. The introduction of ordered channels is thus important for further enhancement of the properties associated with the dendritic/porous nanostructures.[8] To date, ordered porous metal nanostructures have only been obtained using sacrificial hard templates or electrochemical methods.[8,9] To scale up their production, an effective wet-chemical strategy has yet to be identified. If the branches of the porous nanostructures could be oriented in the preferred manner and the branch sizes could be further reduced, superior properties would be obtained.

Palladium (Pd), a key catalyst, plays a central role in many industrial applications.[10] Nanostructured Pd serves as the primary catalyst for various organic reactions and also has remarkable performance in hydrogen storage and hydrogen sensing.[11] All of these applications require precise control over Pd nanostructures to maximize their performance.[12] Herein, we report a convenient and effective wet-chemical strategy that produces uniform porous palladium nanostructures (pPdNs) with perpendicular pore channels. To our knowledge, this is the first time that pPdNs with perpendicular pore channels have been directly prepared in aqueous solution at ambient temperature without the need of premade seed structures, organic solvents, or hard templates. Strikingly, the average branch diameter in the pPdN is measured to be only 2.5 nm, approximately 12 atoms thick. The selection of hexadecylpyridinium chloride (HDPC) as the shape-directing agent is critical to the formation of pPdNs. In addition, new Au@pPd nanstructures can be readily obtained when Au and Pd metal precursors are fed together. More importantly, the obtained pPdNs exhibit better catalytic activity than commercial Pd black and a home-made Pd catalyst for the hydrogenation of nitrobenzene, styrene, and also a Suzuki coupling reaction, making them promising for advanced catalytic applications.

In a typical synthesis of the pPdNs, an aqueous solution of sodium tetrachloropalladate (Na_2PdCl_4) and HDPC were added into a vial. After homogeneous mixing, a freshly prepared aqueous ascorbic acid solution was added quickly under gentle shaking. After the vial was capped, the resulting mixture was kept undisturbed at 35 °C for 3 h. The resulting colloidal product was collected by centrifugation and washed two times with water.

These colloidal products were initially examined by powder X-ray diffraction (PXRD). As shown in Figure S1 a

[*] Dr. X. Huang, Dr. Y. Li, Dr. Y. Chen, Dr. E. Zhou, Prof. Y. Huang
Department of Materials Science and Engineering
University of California-Los Angeles
Los Angeles, 90095 (USA)
E-mail: yhuang@seas.ucla.edu
Dr. Y. Xu, H. Zhou, Prof. X. Duan
Department of Chemistry and Biochemistry
University of California-Los Angeles
Los Angeles, 90095 (USA)
Prof. X. Duan, Prof. Y. Huang
California Nanosystems Institute
University of California-Los Angeles
Los Angeles, 90095 (USA)

[**] We acknowledge the support from ARO, Award 54709-MS-PCS and ONR Award N00014-08-1-0985. We thank EICN at CNSI for the TEM support. Y.H. acknowledges support from the Sloan Research Fellowship.

Supporting information for this article (experimental details) is available on the WWW under http://dx.doi.org/10.1002/anie.201208901.

(in the Supporting Information), the peaks at 40.1°, 46.7°, 68.1°, and 82.1° can be readily indexed to the (111), (200), (220), and (311) reflections of face-centered cubic (fcc) Pd (JCPDS no. 05-0681), indicating metallic Pd crystals. No detectable impurity peaks were observed in the PXRD pattern. In particular, the diffraction peaks were broadened, indicating nanoscale structural features. Representative electron microscopy images of the as-prepared colloidal products are shown in Figure 1. Typical transmission electron microscope (TEM) images show that the product consists of uniform nanostructures with a nearly spherical profile. The nanostructures are highly monodisperse, with sizes narrowly ranging from 78 nm to 86 nm (average of 82 nm) (Figure 1; Figure S1). Importantly, each nanostructure surveyed is of a porous nature with highly branched subunits. Remarkably, the branches of the nanostructures are oriented in a branching-out manner to create perpendicular pore channels between the branches, indicating the successful formation of porous Pd nanostructures (pPdNs). The number of branches on each pPdN ranges up to 30, with an average of 22 branches. The average diameter of the branches is approximately 2.5 nm. The porous nature of the nanoparticles is clearly presented in the high-angle annular dark-field scanning TEM (HAADF-STEM) image (Figure 1c). N_2 adsorption measurements also confirmed the highly porous nature of the pPdNs (Figure S1b). The Brunauer-Emmett-Teller (BET) measurement showed that the pPdNs have a very high surface area of 61.2 $m^2 g^{-1}$. The crystalline nature of the obtained pPdNs was analyzed by selected area electron diffraction (SAED) and high-resolution transmission electron microscope (HRTEM) measurements (Figure 1d,e). The SAED pattern on individual pPdN (inset of Figure 1d) shows concentric rings, composed of bright discrete diffraction spots, which can be indexed to the crystal planes of fcc Pd, indicating the high crystallinity of the pPdNs. The HRTEM image (Figure 1e) also indicates good crystallization of the pPdNs. The clear fringes in the HRTEM image show periods of 0.19 nm and 0.24 nm, as expected for fcc Pd(200) and Pd(111) planes, respectively.

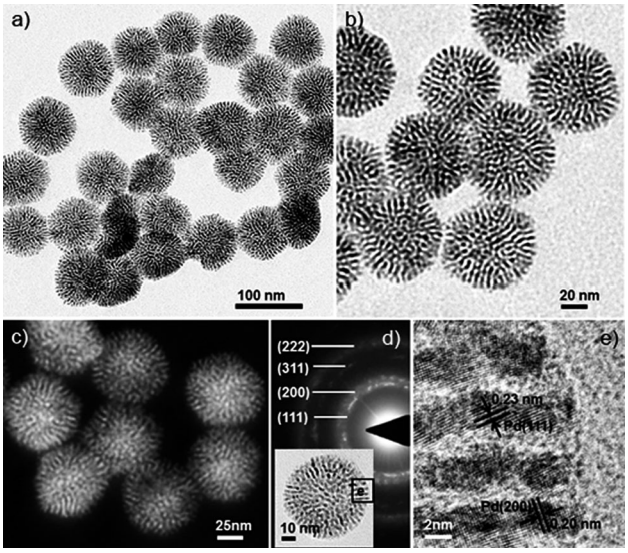

Figure 1. a) Representative low-magnification TEM, b) high-magnification TEM, and c) HAADF-STEM images of as-prepared pPdNs. d) SAED pattern of an individual pPdN. Inset shows the corresponding TEM image with a box around the portion shown in (e). e) HRTEM image of the branches of a pPdN.

The above structural analyses confirm the formation of pPdNs with perpendicular pore channels by wet-chemical synthesis. In contrast to the sacrificial hard-template strategy or electrochemical methods used for the formation of ordered porous metal nanostructures, the synthesis described herein exhibits remarkable efficiency and simplicity, which is highly desirable for practical applications. The resulting pPdNs offer two advantages over previously reported dendritic/porous nanostructures: a) the pPdNs have a higher percentage of surface atoms owing to the reduced diameter of the branches, b) the transport of guest species in the pPdNs can be significantly facilitated by the perpendicular pore channels. The mechanism by which they are grown thus deserves thorough investigation. Through careful time-resolved TEM studies, we found that pPdNs developed at the very beginning of the growth process. Figure 2 shows the morphologies of growth intermediates of pPdNs collected at different reaction times. The pPdNs produced during the first minute of the reaction had an average size of 39 nm. At this initial stage, the porous nanostructures have already started to appear. These nanostructures continued to grow for 15 minutes. The average size of the nanostructures increased to 55 nm at three minutes, to 74 nm at six minutes, and to 81 nm at 15 minutes. During the growth of the nanostructures, their porosity also became more and more prominent with the increasing size of the intermediates. Beyond 15 minutes, no further change in the size or the morphology of the nanostructures was observed (Figure 2e). These results imply that the growth of pPdNs is highly regulated by the reaction system even at the early stages of growth.

In the present synthesis, the selective use of HDPC was critical for the formation of pPdNs. The reaction in the absence of HDPC surfactant resulted in irregular nano-

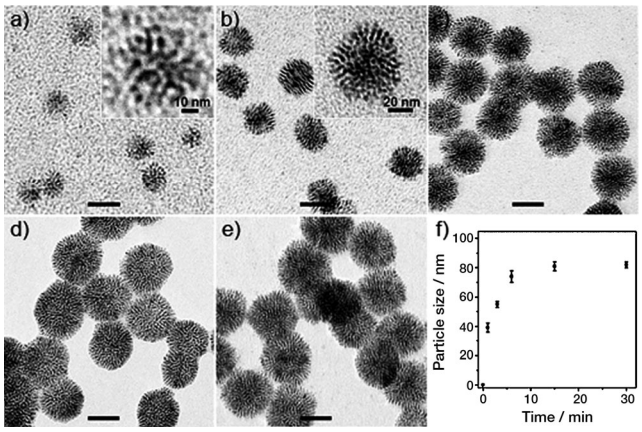

Figure 2. TEM images of the growth intermediates of pPdNs produced after a) 1 min, b) 3 min, c) 6 min, d) 15 min, and e) 30 min. Unlabeled scale bars correspond to 50 nm. f) Changes in the overall particle diameter during the reaction, calculated from the TEM images.

particles (Figure S2 a,b). Moreover, insufficient amounts of HDPC lead to the formation of lower quality pPdNs (Figure S2 c,d). Additionally, when HDPC was replaced with poly(vinyl pyrrolidone) (PVP), small Pd nanoparticles instead of pPdNs formed (Figure S3). When HDPC was replaced with hexadecyltrimethylammonium chloride (CTAC), structures with sizes between 20 nm and 100 nm were obtained. These structures were not as regular as the pPdNs prepared with HDPC and consisted of interconnected Pd nanocrystals and large subunits. We infer that the Pd precursors interact with hexadecylpyridinium cations to form thereon the pPdNs upon the addition of ascorbic acid (Figure S4). Such an interaction is similar to the role of ionic surfactants in directing the formation of ordered mesoporous silica-based materials.[13] HDPC produces pPdNs with higher regularity compared to that of CTAC, mainly because of the special polarizability and compactness of the headgroup.[14] In more controlled syntheses, we found the use of H_2O as a solvent is important to obtain pPdNs with good dispersity and high quality but is not essential for the formation of porous nanostructures. When we replaced H_2O with DMF or ethylene glycol, heavily aggregated porous nanostructures were obtained (Figure S5). The addition of ascorbic acid also played an important role in producing pPdNs with well-defined porous structures. When we substituted ascorbic acid with stronger reducing agents such as hydrazine or sodium borohydride ($NaBH_4$), the pPdNs produced were of lower quality (many heavily aggregated; Figure S6). We propose that ascorbic acid is better for controlling the growth rate of the pPdNs owing to its milder reducing power, which might benefit the formation of uniform porous structures. Overall, the selective use of HDPC as the structure-directing agent, ascorbic acid as the reducing agent, and H_2O as the solvent was responsible for the well-controlled synthesis of pPdNs. Furthermore, the size of the pPdNs is tunable by varying the concentration of ascorbic acid or the reaction temperature. Decreasing the reaction temperature from 35 °C to 20 °C led to an increase in average size from 82 nm to 101 nm (Figure 3). Increasing the reaction temperature to 50 °C produced pPdNs with an average size of 51 nm. Increasing the amount of ascorbic acid used from 0.3 mL to 0.4 mL led to a decrease in average size from 82 nm to 63 nm.

Besides monometallic pPdNs, bimetallic Au@Pd nanostructure with porous Pd shell could be readily synthesized (Figure 4; Figure S7). The procedure for synthesis of porous Au@Pd nanostructures was similar to that of pPdNs, except that $HAuCl_4$ was fed together with Na_2PdCl_4 (Supporting Information). The representative TEM and HAADF-STEM images (Figure 4 a,b) reveal that the products are well-defined porous nanostructures with a solid core, and are uniform in shape and size. The size of the nanostructures varied from 48 nm to 54 nm and averages 51 nm. The inductively coupled plasma atomic-emission spectroscopy (ICP-AES) result suggests that the molar ratio between Au and Pd is 1:3.9. The Au/Pd atomic ratio of the products is in good agreement with the Au/Pd atomic ratio in the initial reaction mixture, implying that all the Au and Pd precursors are reduced in the reaction. Figure 4 c shows the elemental mapping of an individual nanostructure obtained by HAADF-STEM-EDS, which clearly reveals that Pd is distributed throughout the entire nanostructure while Au is concentrated in the core. The PXRD pattern of the products (Figure 4 d) shows two distinct sets of diffraction peaks assigned to the fcc structures of Au and Pd, confirming the formation of metallic Au and Pd in the products. Thus, all the data support the formation of bimetallic porous Au@Pd nanostructures. Together, we have developed a simple and efficient approach to prepare porous Pd-based nanostructures.

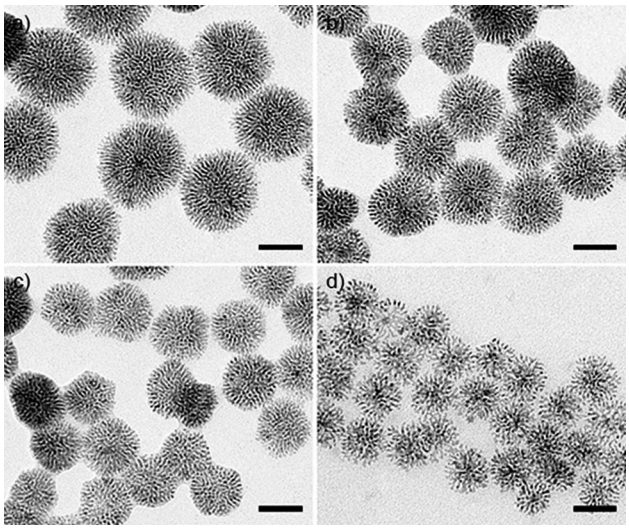

Figure 3. TEM images of pPdNs produced under different reaction conditions: a) room temperature (20 °C), b) 0.3 mL ascorbic acid, c) 0.4 mL ascorbic acid, and d) 50 °C. Other synthesis condition were similar to that of the typical synthesis. Scale bars = 50 nm.

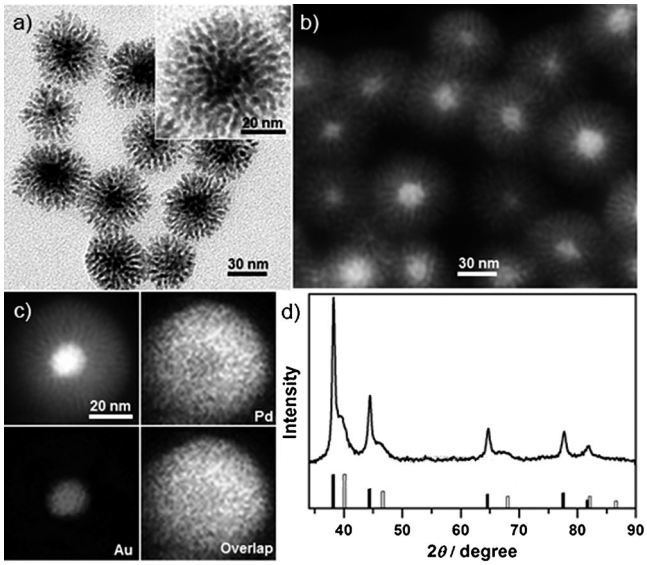

Figure 4. a) Representative low-magnification TEM and b) HAADF-STEM images of as-prepared porous Au@Pd nanostructures. c) HAADF-STEM image and EDX mapping images of a porous Au@Pd nanostructure. d) XRD pattern of the porous Au@Pd nanostructures. Bars show the calculated values for Au (black, JCPDS no. 04-0784) and Pd (gray, JCPDS no. 05-0681).

Owing to their ultrathin subunits and highly open structures, the as-prepared pPdNs have a high percentage of atoms on the surface, and thus are expected to have superior catalytic performance. This type of Pd-based nanomaterials are highly active hydrogenation catalysts.[15] To demonstrate their advantage in catalysis, we chose to examine their use in the hydrogenation of nitrobenzene and styrene. Commercial Pd black, commercial Pd/C and a home-made Pd catalyst (Figures S8,9, Table S1) were used as references for comparison. In a typical hydrogenation of nitrobenzene, nitrobenzene was converted into aniline using hydrogen gas over the Pd catalysts. Ethanol was used as the solvent. Figure 5a compares the formation of reaction products against time after the addition of the catalysts for the hydrogenation of nitrobenzene. After the addition of the pPdNs, the hydrogenation reaction proceeds very fast, with nearly 100% conversion of nitrobenzene and approaching 100% selectivity to aniline was achieved within only 90 minutes. However, under the same catalysis conditions described above while replacing the pPdNs with the same amount of commercial Pd black, only 38.1% of nitrobenzene was converted during the 90 minute reaction, and only 55.7% for the home-made Pd catalysts. Similar behavior was also found for the hydrogenation of styrene (Figure 5b), for which the pPdNs showed activity that was 3.1- and 2.1-times greater than those of commercial Pd black and home-made Pd catalyst, respectively (based on the conversion at 60 minutes). The activity of pPdNs for hydrogenation of both nitrobenzene and styrene is also comparable to the highly supported commercial Pd/C (Figure 5a,b; Table S2).

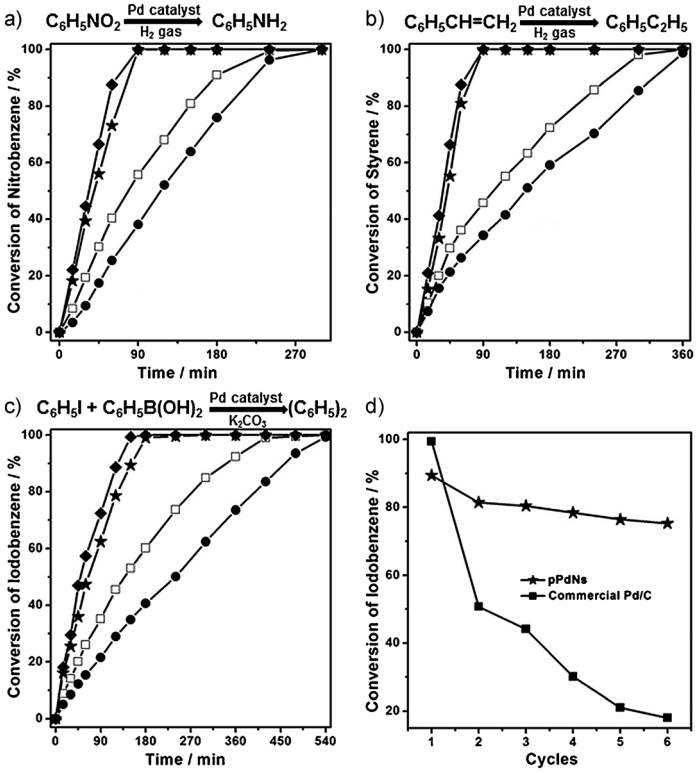

Figure 5. Conversion of a) nitrobenzene and b) styrene during hydrogenation reactions and c) iodobenzene during the Suzuki coupling reaction catalyzed by different Pd catalysts; pPdNs (★), home-made Pd (□), commercial Pd black(●), commercial Pd/C (◆). d) A comparison of conversion for pPdNs and Pd/C during the six Suzuki-coulpling reaction cycles. The reaction time is 150 min.

In addition to their excellent activity for the hydrogenation of nitrobenzene and styrene, the pPdNs also showed high catalytic performance in the Suzuki coupling reaction. In a typical catalytic reaction (see Supporting Information for details), phenylboronic acid was coupled with iodobenzene to form biphenyl over Pd catalysts at 60 °C. Ethanol was used as the solvent. The concentration by weight of Pd in solution was kept the same for all the Pd catalysts. Figure 5c shows rate of Suzuki coupling for the different Pd catalysts. For the pPdNs, 99.1% of the iodobenzene is converted into biphenyl after 180 minutes. In comparison, a yield of 40.7% for commercial Pd black and 60.1% for home-made Pd catalyst was obtained in the same time. Based on the conversion at 180 minutes, the activity of the pPdNs was 2.43- and 1.65-times higher than that of the commercial Pd black and home-made Pd catalyst, respectively. The activity of pPdNs for the Suzuki coupling is comparable to the same weight percent Pd of commercial Pd/C. However, the pPdNs showed far better stability during cycles of the Suzuki coupling reaction (Figure 5d). There was only a slight decrease in the percent conversion between the reused and fresh pPdNs catalysts after six cycles. In contrast, an obvious decrease in activity is observed for the commercial Pd/C (Figure 5d). TEM measurements revealed that after multiple catalytic reactions, the pPdNs largely maintained their morphologies (Figure S10). In comparison, under the same conditions, the commercial Pd/C catalysts showed serious ripening and aggregation, highlighting the improved structural stability of the pPdNs. Together, our studies clearly demonstrate that the prepared pPdNs show excellent catalytic activity and reusability (Table S2), which opens up the possibility for other important applications, such as hydrogen storage and hydrogen sensing.

In summary, we have developed an efficient synthesis of Pd-based porous nanostructures featuring well-defined perpendicular pore channels and ultrathin branches. This synthesis takes place in an aqueous phase under mild conditions without using a hard template, which differentiates it from previous reported methods. The manner of the growth and the roles of each of the reagents were fully explored. It was demonstrated that the pPdNs can serve as highly efficient catalysts for hydrogenation reactions and a Suzuki coupling reaction, where they outperformed commercial Pd black and home-made Pd dendrites. More importantly, the pPdNs showed similar catalytic performance to highly supported commercial Pd/C but with far better stability. This high catalytic performance can be attributed to the high surface area and perpendicular dendritic structures in the pPdNs that provide highly accessible surface active sites, as well as maintain the structural integrity of the catalysts.

Received: November 7, 2012
Revised: December 4, 2012
Published online: January 30, 2013

Keywords: hydrogenation · nanostructures · palladium · porous materials · Suzuki coupling

[1] a) T. S. Ahmadi, Z. L. Wang, T. C. Green, A. Henglein, M. A. El-Sayed, *Science* **1996**, *272*, 1924 – 1926; b) B. Lim, M. J. Jiang, P. H. C. Camargo, E. C. Cho, J. Tao, X. M. Lu, Y. M. Zhu, Y. N. Xia, *Science* **2009**, *324*, 1302 – 1305; c) V. R. Stamenkovic, B. Fowler, B. S. Mun, G. F. Wang, P. N. Ross, C. A. Lucas, N. M. Markovic, *Science* **2007**, *315*, 493 – 497; d) S. E. Habas, H. Lee, V. Radmilovic, G. A. Somorjai, P. Yang, *Nat. Mater.* **2007**, *6*, 692 – 697; e) C. Y. Chiu, Y. J. Li, L. Y. Ruan, X. C. Ye, C. B. Murray, Y. Huang, *Nat. Chem.* **2011**, *3*, 393 – 399.

[2] a) M. C. Daniel, D. Astruc, *Chem. Rev.* **2004**, *104*, 293 – 346; b) M. A. Newton, *Chem. Soc. Rev.* **2008**, *37*, 2644 – 2657; c) A. C. Chen, P. Holt-Hindle, *Chem. Rev.* **2010**, *110*, 3767 – 3804.

[3] a) A. Morozan, B. Jousselme, S. Palacin, *Energy Environ. Sci.* **2011**, *4*, 1238 – 1254; b) Z. M. Peng, H. Yang, *Nano Today* **2009**, *4*, 143 – 164.

[4] a) K. M. Bratlie, H. Lee, K. Komvopoulos, P. D. Yang, G. A. Somorjai, *Nano Lett.* **2007**, *7*, 3097 – 3101; b) C. Wang, H. Daimon, T. Onodera, T. Koda, S. H. Sun, *Angew. Chem.* **2008**, *120*, 3644 – 3647; *Angew. Chem. Int. Ed.* **2008**, *47*, 3588 – 3591; c) R. Narayanan, M. A. El-Sayed, *J. Am. Chem. Soc.* **2004**, *126*, 7194 – 7195.

[5] Y. N. Xia, Y. J. Xiong, B. Lim, S. E. Skrabalak, *Angew. Chem.* **2009**, *121*, 62 – 108; *Angew. Chem. Int. Ed.* **2009**, *48*, 60 – 103.

[6] a) B. Lim, Y. N. Xia, *Angew. Chem.* **2011**, *123*, 78 – 87; *Angew. Chem. Int. Ed.* **2011**, *50*, 76 – 85; b) J. Y. Chen, B. Lim, E. P. Lee, Y. N. Xia, *Nano Today* **2009**, *4*, 81 – 95.

[7] a) F. Wang, C. H. Li, L. D. Sun, C. H. Xu, J. F. Wang, J. C. Yu, C. H. Yan, *Angew. Chem.* **2012**, *124*, 4956 – 4960; *Angew. Chem. Int. Ed.* **2012**, *51*, 4872 – 4876; b) X. Q. Huang, S. H. Tang, J. Yang, Y. M. Tan, N. F. Zheng, *J. Am. Chem. Soc.* **2011**, *133*, 15946 – 15949; c) Z. M. Peng, H. Yang, *J. Am. Chem. Soc.* **2009**, *131*, 7542 – 7543; d) L. Wang, Y. Yamauchi, *J. Am. Chem. Soc.* **2009**, *131*, 9152 – 9153; e) M. A. Mahmoud, C. E. Tabor, M. A. El-Sayed, Y. Ding, Z. L. Wang, *J. Am. Chem. Soc.* **2008**, *130*, 4590 – 4591; f) A. Mohanty, N. Garg, R. C. Jin, *Angew. Chem.* **2010**, *122*, 5082 – 5086; *Angew. Chem. Int. Ed.* **2010**, *49*, 4962 – 4966; g) T. Soejima, N. Kimizuka, *J. Am. Chem. Soc.* **2009**, *131*, 14407 – 14412.

[8] a) Y. Yamauchi, A. Takai, T. Nagaura, S. Inoue, K. Kuroda, *J. Am. Chem. Soc.* **2008**, *130*, 5426 – 5427; b) A. H. Lu, F. Schuth, *Adv. Mater.* **2006**, *18*, 1793 – 1805.

[9] a) Y. Yamauchi, A. Tonegawa, M. Komatsu, H. J. Wang, L. Wang, Y. Nemoto, N. Suzuki, K. Kuroda, *J. Am. Chem. Soc.* **2012**, *134*, 5100 – 5109; b) A. Takai, Y. Yamauchi, K. Kuroda, *J. Am. Chem. Soc.* **2010**, *132*, 208 – 214.

[10] a) Y. Nishihata, J. Mizuki, T. Akao, H. Tanaka, M. Uenishi, M. Kimura, T. Okamoto, N. Hamada, *Nature* **2002**, *418*, 164 – 167; b) F. Favier, E. C. Walter, M. P. Zach, T. Benter, R. M. Penner, *Science* **2001**, *293*, 2227 – 2231.

[11] a) S. W. Kim, M. Kim, W. Y. Lee, T. Hyeon, *J. Am. Chem. Soc.* **2002**, *124*, 7642 – 7643; b) M. S. Jin, H. Zhang, Z. X. Xie, Y. N. Xia, *Angew. Chem.* **2011**, *123*, 7996 – 8000; *Angew. Chem. Int. Ed.* **2011**, *50*, 7850 – 7854.

[12] Y. J. Xiong, Y. N. Xia, *Adv. Mater.* **2007**, *19*, 3385 – 3391.

[13] Y. Wan, D. Y. Zhao, *Chem. Rev.* **2007**, *107*, 2821 – 2860.

[14] D. B. Kuang, T. Brezesinski, B. Smarsly, *J. Am. Chem. Soc.* **2004**, *126*, 10534 – 10535.

[15] G. A. Somorjai, Y. M. Li, *Top. Catal.* **2010**, *53*, 832 – 847.

